# Closed-Loop Dynamic Stall Control Using a Stall-Warning Sensor

**Preprint** · March 2025

CITATIONS
0

READS
7

**3 authors**, including:

David Greenblatt
Technion – Israel Institute of Technology
**202** PUBLICATIONS **5,411** CITATIONS

SEE PROFILE

# Closed-Loop Dynamic Stall Control Using a Stall-Warning Sensor

Mordechai Garcia,[*]

*Technion – Israel Institute of Technology, Technion City, Haifa 3200003, Israel*

Michael Mongin[†]

*U.S. Air Force Research Laboratory, Wright-Patterson Air Force Base, OH 45433, USA*

David Greenblatt[‡]

*Technion – Israel Institute of Technology, Technion City, Haifa 3200003, Israel*

## Nomenclature

| | | |
|---|---|---|
| $AR$ | = | aspect ratio, $b/\bar{c}$ |
| $b/2$ | = | wing semi-span (m) |
| $\bar{c}$ | = | average wing chord (m) |
| $C_D$ | = | wing drag coefficient, $F_D / q_\infty S$ |
| $C_L$ | = | wing lift coefficient, $F_L / q_\infty S$ |
| $f$ | = | wing oscillation frequency (Hz) |
| $f_p$ | = | perturbation frequency, $1/T_p$ (Hz) |
| $F^+$ | = | reduced perturbation frequency, $f_p \bar{c} / U_\infty$ |
| $k$ | = | reduced wing oscillation frequency, $\omega \bar{c} / 2U_\infty$ |
| $q_\infty$ | = | dynamic pressure, $\frac{1}{2}\rho U_\infty^2$ (Pa) |
| $Re$ | = | Reynolds number, $U_\infty \bar{c} / \nu$ |
| $S$ | = | wing planform area ($m^2$) |
| $U_\infty$ | = | wind tunnel freestream velocity (m/s) |

[*] Graduate Student, Faculty of Mechanical Engineering.
[†] Aerospace Researcher, Aerospace Systems Directorate, AIAA Young Professional Member.
[‡] Professor, Louis and Helen Rogow Chair in Aeronautical Engineering. Faculty of Mechanical Engineering, AIAA Associate Fellow, davidg@technion.ac.il (corresponding author).

$V_{pp}$ = peak-to-peak voltage (kV)

$\alpha$ = angle-of-attack (°)

$\alpha_s$ = stall angle-of-attack (°)

$\omega$ = wings circular oscillation frequency (rad/s)

# I. Introduction

The introduction of periodic perturbations at the leading-edges of airfoils and wings is known to be effective for flow separation control under incompressible and compressible subsonic conditions [1,2]. The control of flow separation—also called stall control—can reduce stall speed, increase endurance and improve flight safety [3]. Typical effective reduced perturbation frequencies are $F^+ = \mathcal{O}(1)$, but they can be as high as $F^+ = \mathcal{O}(10^2)$ [4,5]. Under conditions of unsteady pitching, that lead to dynamic stall, the introduction of periodic perturbations is effective when $f_p \gg f$, i.e., $F^+ \gg k/\pi$ [6]. This inequality covers a wide range of relevant engineering problems, including rotary-wing aircraft, wind turbines, and small unmanned air vehicles exposed to gusts. It is self-evident that perturbations only need to be initiated when the airfoil or wing approaches, or is at, the static stall angle—and this involves some form of closed-loop control.

A closed-loop DBD plasma control scheme was developed by [7] based on measuring the upper surface pressure signal downstream $(x/c = 8\%)$ of the actuator. The actuator was operated at a low-amplitude pulsation mode—designed to amplify disturbances at incipient stall—and then switched to a high-amplitude separation control mode when some bandpass filtered threshold was exceeded. In a different approach, flush-mounted microphones near the upper surface trailing-edge of an airfoil were used to detect incipient separation by [8]. A far older and simpler way of detecting incipient stall is based on downstream stagnation-point movement just below the leading-edge [9]. In a typical application, the resulting negative air pressure sucks air through a reed, producing an audible stall-warning, thereby allowing the pilot to take corrective action. An obvious extension to this is to adapt a conventional stall warning system to either initiate or terminate leading-edge perturbations. The objective of this Technical Note is to evaluate the adaptation of such a system under conditions of dynamic stall for both harmonic pitching and pitch-and-hold motions.

## II. Experimental Setup

Experiments were performed on a semi-span wing in a blow-down wind tunnel, with a 1.0 × 1.9 m test section, a maximum wind speed of $U_\infty = 16$ m/s, a maximum flow distortion of 2.5% and a maximum turbulence intensity of 0.5%. The wind tunnel speed was measured using a pitot-static probe, mounted upstream of the model, using a Siemens QBM3020-1U pressure transducer, together with an E+E Elektronik EE211 humidity and temperature sensor. The wing was constructed from expanded polyolefin (EPO), with a constant chord-length inboard (root) section, a mildly tapered outboard section, and drooped wingtips (see Fig. 1). It is based on a 6:1 Cessna 172 wing planform, with a semi-span (not including the model body) of 1.62 m and GOE 702 airfoil geometry, whose thickness is scaled by a factor of 0.6702. A leading-edge pressure port was installed below the leading-edge at $x/c = 0.32\%$ (see Fig. 1, top-right), and connected to a Honeywell HSC 250 pascal differential pressure sensors, whose static line was connected to tunnel static line. DBD plasma actuators consisting of 50 μm thick copper electrodes and a 0.4 mm thick silicone rubber dielectric, were mounted along the full extent of the span. High-voltage signals were supplied using a Minipuls 0.1® (GBS Elektronik) generator at 12-kV peak-to-peak and 9.65 kHz, with a pulse-modulation (or perturbation) frequency of $f_p = 110$ Hz $(F^+ = 3.3)$ and a duty cycle $\text{d.c.} = 15\%$. The voltage was monitored using a Testec ESTEC HVP-15HF high voltage probe. All experiments were performed at $U_\infty = 8.5$ m/s $(Re = 1.46 \times 10^5)$, which corresponded to the flight model stall speed [3].

The wing was mounted horizontally in the test section on a 20×80 mm aluminum profile, incorporating a stainless-steel shaft mounted on bearings, a six-component ATI Delta SI-330-30 aerodynamic balance, an extension, a lever-arm and a wing adapter (see Fig. 1). A Nema 17 stepper motor was also fixed to the aluminum profile and attached to the shaft via a timing belt, to produce a step resolution of 0.014 degrees. The pitch angle was measured using a Singer Instruments Model MTS-D inclinometer. To mitigate wall boundary layer effects, the wing was located 15 cm from the test section wall, and an 80×80 cm Plexiglas endplate placed at approximately 1.5 mm from the wing root. For both static and dynamic pitching experiments, wind-off (tare) load measurements were accounted for.

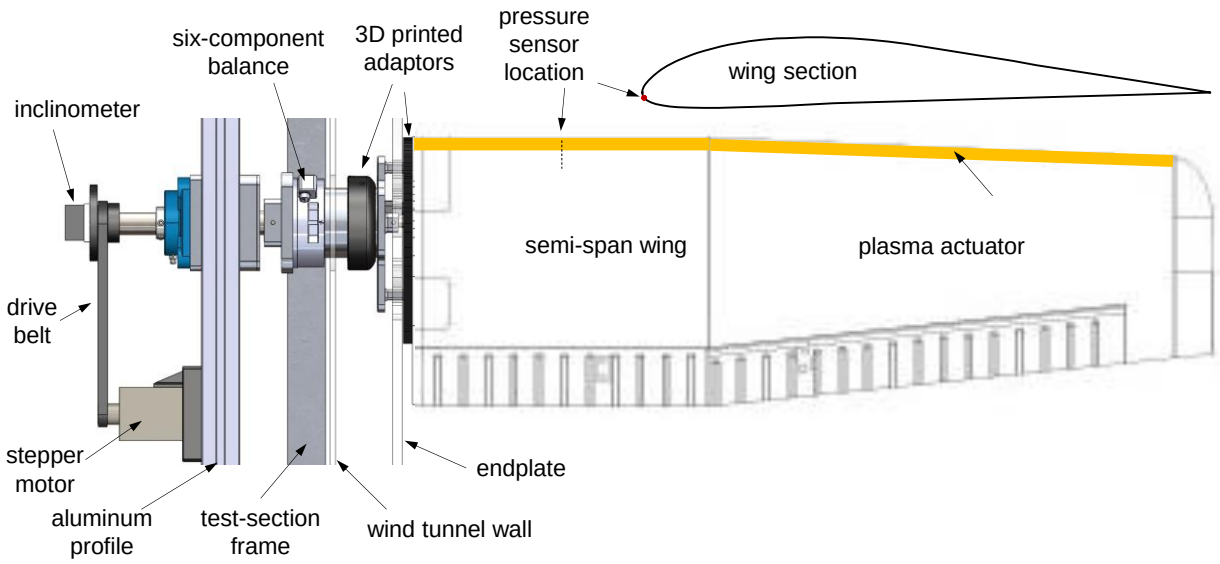


**Fig. 1. Top view schematic of the cantilever setup, showing the main assembly components required for dynamically pitching the wing, while measuring the loads and pitch angle. Top-right: scaled GOE 702 airfoil geometry indicating the stall warning sensor location.**

## III. Discussion of Results

### A. Static Load Data and Sensing

Static aerodynamic coefficient and leading-edge pressure results are shown in Fig. 2 for both baseline and plasma perturbation cases. The perturbations produced results comparable to those found in the literature, and although $F^+ = 3.3$ did not produce the largest post-stall $C_L$ improvements [3], it was selected because perturbations at $F^+ \approx 1$ produced relatively large flapping vibrations of the wing. A comparison between the lift coefficient and leading-edge pressure indicated a pressure zero-crossing at approximately half a degree beyond $\alpha_s$ and was therefore more of a stall indicator than a stall warning. However, placing a pressure port further upstream proved to be impractical due to the presence of the actuator's exposed electrode. Nevertheless, due to the near correspondence of the zero-crossing and the static stall angle, the sensor placement was deemed suitable for implementation in a simple closed-loop system, based on the threshold setting $p_t = 0$. For implementation purposes, measured pressure signals were averaged in 50 ms windows to obtain $\Delta p$, and the following simple logic was applied: if $\Delta p \le p_t$, then perturbations were initiated; if $\Delta p > p_t$, then perturbations were terminated.

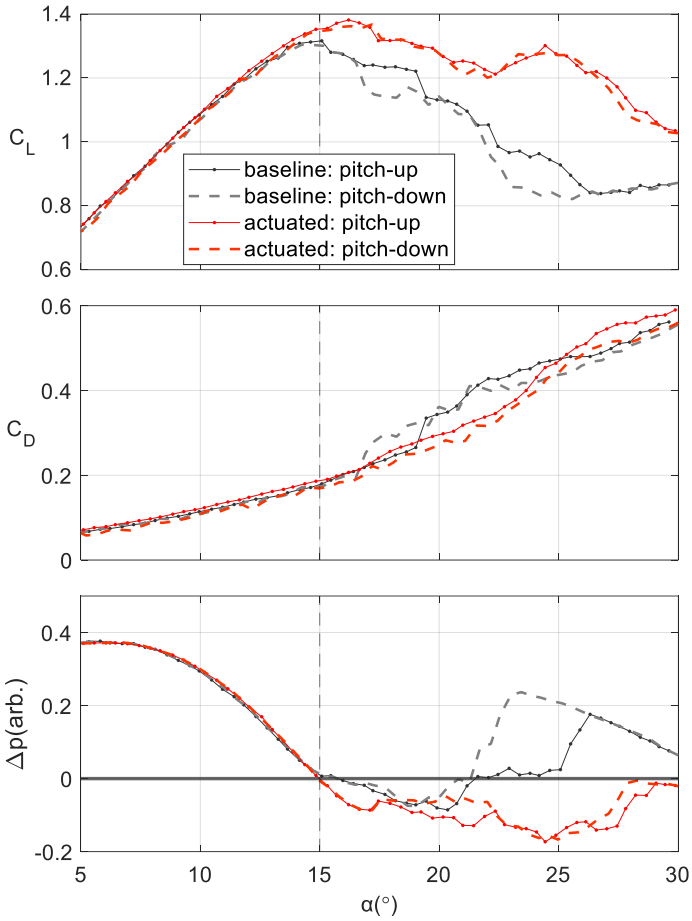


**Fig. 2. Lift and drag coefficient results, together with corresponding leading-edge pressure under static pitch-up and pitch-down motions, for baseline and continuously pulse-modulated (open-loop) cases.**

### B. Unsteady Harmonic Pitching

Harmonic pitching was conducted under the conditions $\alpha = \bar{\alpha} + 5° \sin \omega t$, at low, intermediate and high dimensionless pitchrates: $k = 0.01$, 0.05 and 0.1, respectively; and under light stall $(\bar{\alpha} = 12°,\ \alpha_{\max} = \alpha_s + 2°)$, moderate stall $(\bar{\alpha} = 15°,\ \alpha_{\max} = \alpha_s + 5°)$, and deep stall $(\bar{\alpha} = 18°,\ \alpha_{\max} = \alpha_s + 8°)$. Each experiment included a minimum of 10 cycles, which were subsequently phase-averaged and subtracted from the tare data to produce the net aerodynamic loads. Real-time control was not implemented, and this resulted in a 20 to 50 millisecond deadtime between zero pressure crossings and initiation or termination of the perturbations.

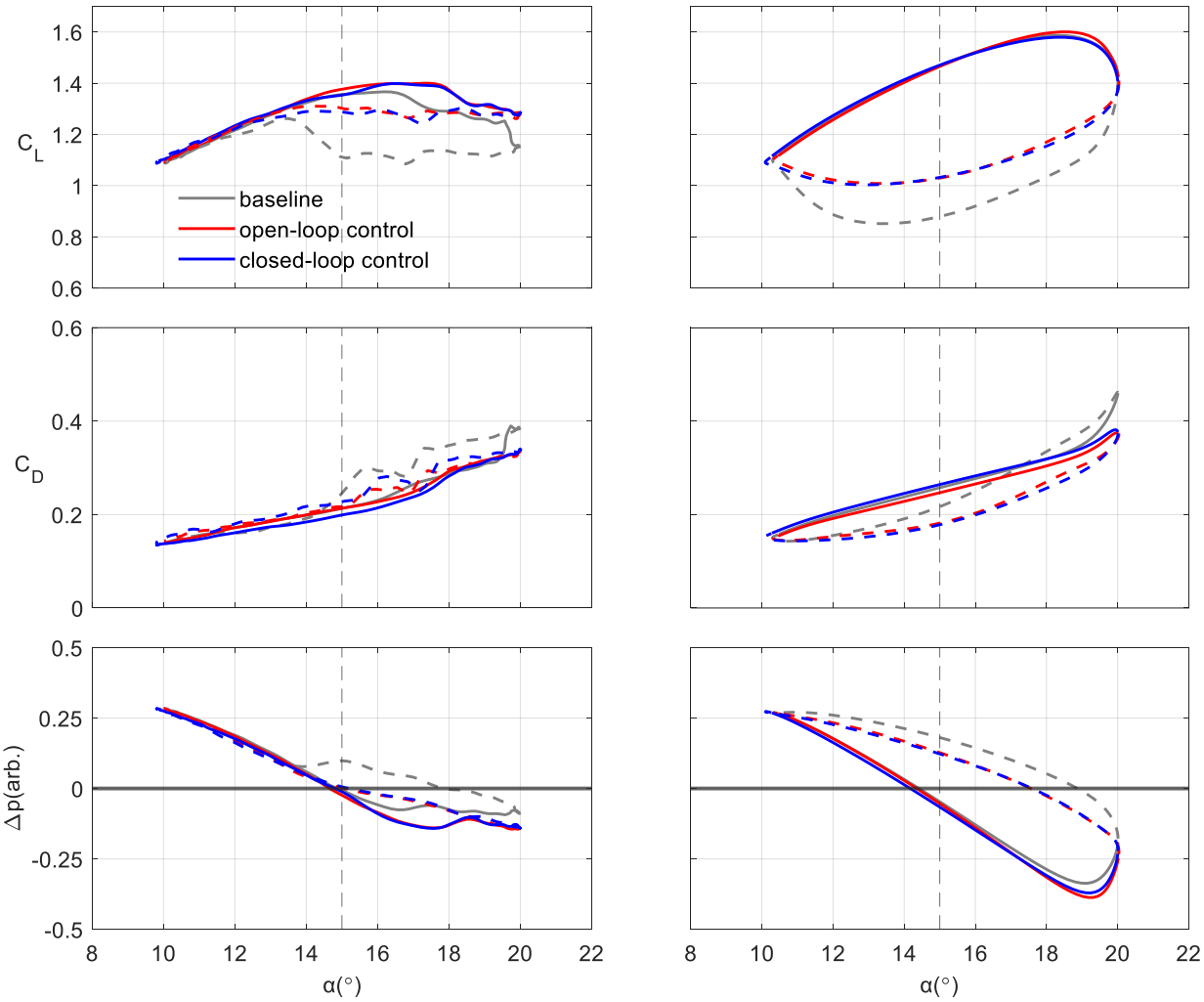


**Fig. 3. Phase-averaged baseline, open-loop and closed-loop aerodynamic coefficients and leading-edge pressure with $\bar{\alpha} = 15°$ at $k = 0.01$ (left) and $k = 0.1$ (right).**

Phase-averaged results at low and high pitchrates are shown in Fig. 3, and light and deep stall results are shown in Fig. 4. For the most part, the open- and closed-loop results are similar, with only minor differences between the pitch-up and pitch down motions. In both cases, perturbations generally decreases the hysteresis loops, consistent with prior airfoil and wing studies [5,10-12], producing higher $C_L$ and lower $C_D$ during the downstroke. The main difference between closed- and open-loop control occurs close to the static stall angle during the pitch-up motion. This is most clearly seen at the lowest pitch rate in Fig. 3 (left-hand column) and is a direct consequence of pulsation initiation at an angle slightly greater than the stall angle. At higher pitchrates, namely

$k = 0.05$ and $k = 0.1$, this difference becomes negligible, due to the delayed response of the boundary layer separation, relative to the time-scales associated with the pitching motion.

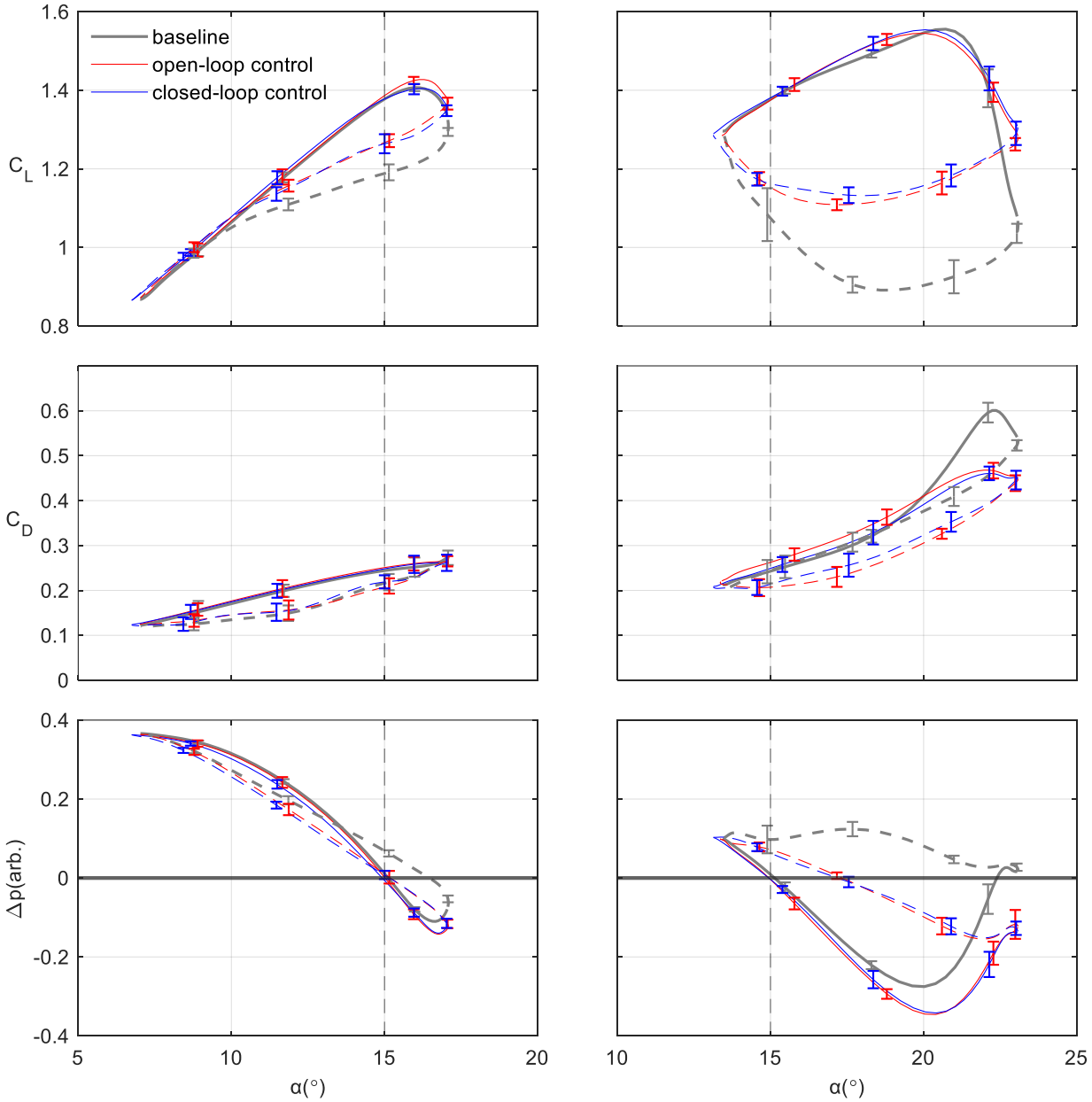


**Fig. 4. Phase-averaged baseline, open-loop and closed-loop aerodynamic coefficients with $\bar{\alpha} = 12°$ (left) and $\bar{\alpha} = 18°$ (right) at $k = 0.05$. Error bars at representative locations show the measurement precision with 95% confidence intervals ($\bar{C} \pm 2\sigma_C / \sqrt{N}$ 95% CI).**

Note, however, that the angles-of-attack corresponding to the pressure zero-crossings during the pitch-down motion increase with increasing pitchrate and angle-of-attack (Fig. 3 and Fig. 4). This means that closed-loop pulsations are terminated at angles-of-attack that are larger than the static stall angle. Despite this, the lift and drag coefficients are essentially identical to those obtained with open-loop control. This is not due to the system dead-time, because dead-time accounts for angles-of-attack of less than one degree. The explanation is as follows: Boundary layer separation following the termination of perturbations occurs over more than 10 convective time units, i.e., $T_{sep}U_\infty / \bar{c} > 10$ [6]. This dimensionless time is comparable to the downstroke ½-cycles for $k = 0.05$ and $k = 0.1$, i.e., $T_{1/2}U_\infty / \bar{c} = \pi / 2k$, which are 31 and 16, respectively. We note from Fig. 3 and Fig. 4 that the downstroke zero-crossings occur at $\alpha = 17.2°$ and 17.5°, and we can readily calculate the dimensionless times between the those angles and $\alpha_s$, namely 4.5 and 2.7, respectively. These dimensionless times are both significantly less than the dimensionless timescales governing flow separation following the termination of perturbations, and the wing returns to pre-stall angles-of-attack well before the boundary layer has a chance to separate. This, then, explains why there is very little difference between the open- and close-loop results. Note, furthermore, that as the pitching frequency increases, the zero-crossing angles increase slightly, but simultaneously the dimensionless times between the zero-crossings and $\alpha_s$ decrease proportionally.

The observations described above demonstrate that leading-edge pressure sensing for closed-loop control furnishes built-in compensation under successively increasing pitching frequencies. This is because for both pitch-up and pitch-down motions, the time-scales governing flow separation are significantly larger than those during which perturbations are not active at post-stall angles-of-attack. This time-scale disparity was exploited during dynamic stall on the blades of a vertical axis wind turbine with leading-edge DBD plasma actuators [13]. It was shown that continuous (open-loop) and limited-azimuth scheduled (feed-forward) post-stall perturbations produced similar turbine performance. The shortening of the active post-stall perturbation time interval—i.e., the smaller fraction of the azimuth that the perturbations were activated—allowed the attainment of a net turbine power gain.

An uncertainty analysis was carried out, based on the number of cycles, $N$, where $\sigma_C$ is the standard deviation associated with each phase-averaged lift or drag coefficient $C$. Uncertainties

based on 95% confidence intervals ($C \pm 2\sigma_C / \sqrt{N}$ 95% CI), are shown for representative points. Note that these uncertainties are conservative because they do not take into account the time-window averaging of the raw lift and drag data. As expected, smaller uncertainties are associated with the pre-static-stall, nominally attached-flow angles-of-attack. A summary of all experiments— low, intermediate and high dimensionless pitchrates; and light, moderate and deep stall—showed that the root-mean-square of the differences between corresponding open-loop and closed-loop lift coefficients were always less than 0.025, and primarily a result of experimental error [14].

### C. Unsteady Pitch-and-Hold

Pitch-and-hold experiments were performed by employing half-sine-waves, phased-shifted by $\pi/2$, followed by a constant angle-of-attack, using the identical $\alpha$ and $k$ ranges as for harmonic pitching (described in section III.B). Representative ensemble-averaged results, under moderate stall at the three pitchrates are shown in Fig. 5. For all stall scenarios and pitchrates, open- and closed-loop results were virtually indistinguishable, to within experimental uncertainty, and hence the discussions relating to cases with pulsed-plasma perturbations applies to both. As expected, higher pitch-up rates resulted in greater overshoot of the static maximum lift, and perturbations had a successively smaller effect on the maximum. The accompanying successively lower leading-edge pressures, at corresponding angles, are consistent with greater local inboard circulation.

For the moderate stall (and deep stall, not shown) scenarios, pitch-down produced a lift "undershoot" at the two higher baseline pitchrates. The source of this undershoot is most likely the generation of a leading-edge vortex, that subsequently forms a stagnation region on the upper surface. Similar observations were made on a deflected flap following the initiation of zero mass-flux perturbations [6]. It can be hypothesized that this is, at least in part, a non-circulatory unsteady contribution to lift, due to the weak circulatory response associated with the leading-edge pressures. The formation of the vortex is eliminated by the perturbations at $k = 0.05$ (Fig. 5, center), but at $k = 0.1$ it is not. Without surface pressure or flowfield measurements any attempt to explain these observations is purely speculative, although the dominant factor is the leading-edge initial condition prior to the pitch-down motion. Surface pressure and flowfield measurements—for example particle image velocimetry—would be required to better understand these loading phenomena.

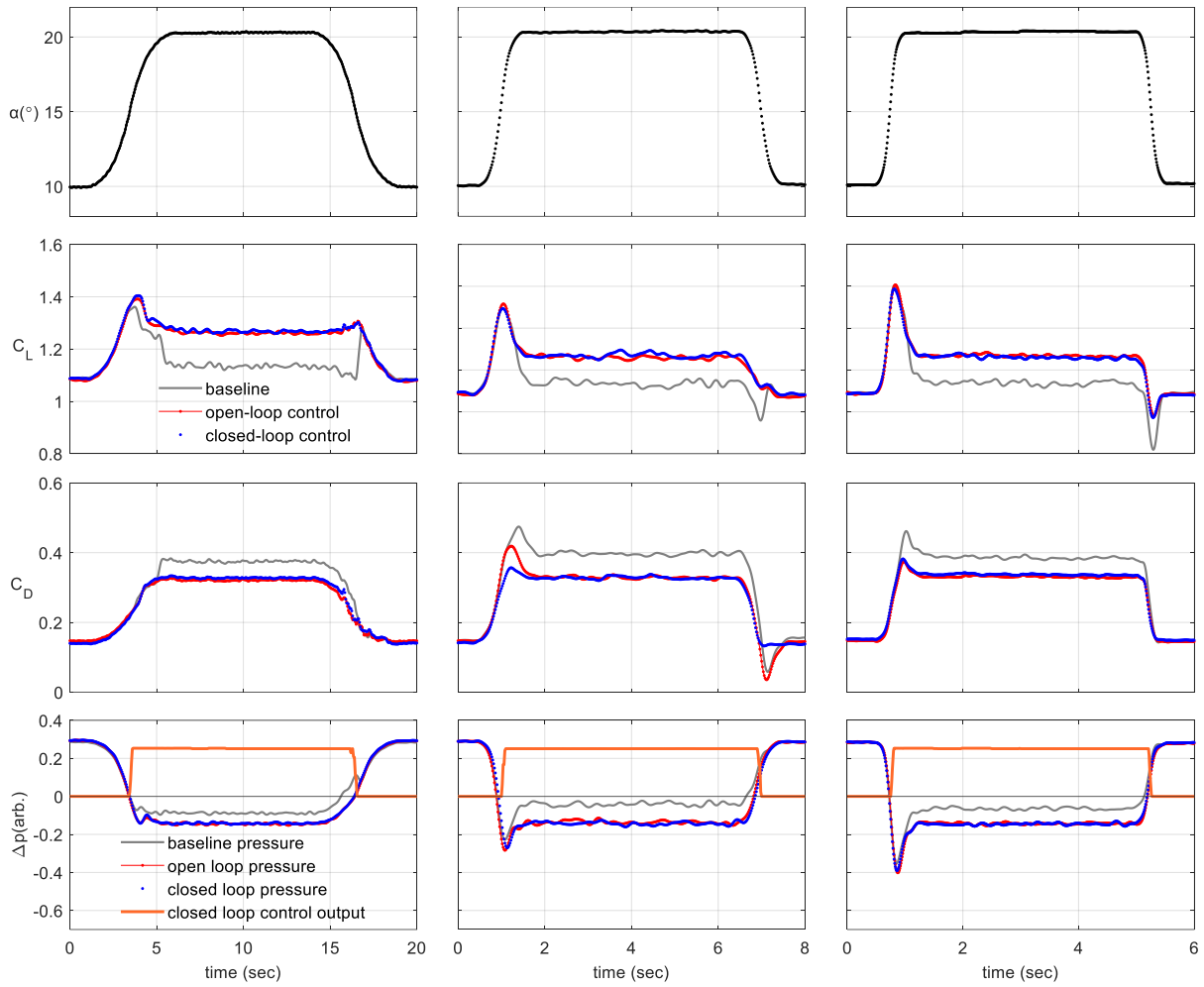


**Fig. 5. Summary of moderate stall pitch-and-hold ensemble-averaged results for $k = 0.01$ (left), $k = 0.05$ (center), and $k = 0.1$ (right).**

## IV. Conclusions

A closed-loop DBD plasma dynamic stall control system was demonstrated in a wind tunnel on a scale-model wing, based on pressure sensing below the leading-edge to initiate or terminate pulse-modulated perturbations. A wide range of angles-of-attack, from light-stall to deep-stall, was considered at reduced frequencies between 0.01 and 0.1, for both periodic sinusoidal and pitch-and-hold motions. The evaluation was conducted by comparing open-loop (continuous pulse-modulation) and closed-loop lift and drag coefficient. For all conditions considered, the differences between open- and closed-loop coefficients were small and ascribed to experimental error, thereby demonstrating the effectiveness and robustness of the system.

A welcome result was that even when pulsations were initiated and terminated at post-static-stall angles during pitch-up and down motions, no meaningful differences between open- and closed-loop control were observed. The reason for this is that the process of flow separation occurred over a significantly larger time than that for which the perturbations are inactive. With increases in pitching frequency, simultaneous increases in the zero-crossing angles and decrease in the time between the pressure zero-crossings and $\alpha_s$ during pitch-down motion, ensures that the method remains effective.

## References


1. Greenblatt, D. and Wygnanski, I., "The control of separation by periodic excitation," *Progress in Aerospace Sciences*, Volume 36, Issue 7, 2000, pp. 487-545. https://doi.org/10.1016/S0376-0421(00)00008-7.
2. Kelley, C.L., Bowles, P.O., Cooney, J., He, C., Corke, T.C., Osborne, B.A., Silkey, J.S. and Zehnle, J., "Leading-edge separation control using alternating-current and nanosecond-pulse plasma actuators," *AIAA Journal*, Vol. 52, No. 9, 2014, pp. 1871-1884. https://doi.org/10.2514/1.J052708
3. Garcia M. and Greenblatt, D., "Mini UAV with DBD-plasma-based flow control," Paper No. 2023-4306, AIAA Aviation Forum, 12-16 June 2023, San Diego, CA. https://doi.org/10.2514/6.2023-4306
4. Visbal, M.R. and Benton, S.I., "Exploration of High-Frequency Control of Dynamic Stall Using Large-Eddy Simulations," *AIAA Journal*, Vol. 56, No. 8, 2018, pp. 2975-2991. https://doi.org/10.2514/1.J056720.
5. De Troyer, T., Hasin, D., Keisar, D., Santra, S. and Greenblatt, D., "Plasma-based dynamic stall control and modelling on an aspect-ratio-one wing," *AIAA Journal* Vol. 60, No. 5, 2022, pp. 2905-2915. https://doi.org/10.2514/1.J060933.
6. Greenblatt, D., Nishri, B., Darabi, A. and Wygnanski, I., "Dynamic stall control by periodic excitation, Part 2: Mechanisms," *Journal of Aircraft*, Vol. 38, No. 3, 2001, pp. 439-447. https://doi.org/10.2514/2.2811.

7. Lombardi, A.J., Bowles, P.O. and Corke, T.C., "Closed-loop dynamic stall control using a plasma actuator," *AIAA Journal*, Vol. 51, No. 5, 2013, pp. 1130-1141. https://doi.org/10.2514/1.J051988.
8. Morice, S.D., Ginnell, K., Geary, S., Baughn, J. and Robinson, S.K., "Detection of boundary layer separation and implementation of autonomous vortex generators," AIAA Paper No. 2020-0788. AIAA Scitech Forum, 6-10 January 2020, Orlando, FL. https://doi.org/10.2514/6.2020-0788.
9. Zalovcik, J.A., "Summary of stall-warning devices," NACA-TN-2676, 1952.
10. Post, M.L. and Corke, T.C., "Separation control using plasma actuators: dynamic stall vortex control on oscillating airfoil, *AIAA Journal*, Vol. 44, No. 12, 2006, pp. 3125-3135. http://dx.doi.org/10.2514/1.22716.
11. Greenblatt, D. and Wygnanski, I., "Dynamic stall control by periodic excitation. Part 1: NACA 0015 Parametric Study," *Journal of Aircraft*, Vol. 38, No. 3, 2001, pp. 430-438. https://doi.org/10.2514/2.2810.
12. Greenblatt, D., "Active control of leading-edge dynamic stall," *International Journal of Flow Control*, Vol. 2, No. 1, 2010, pp. 21-38. http://dx.doi.org/10.1260/1756-8250.2.1.21.
13. Ben-Harav, A. and Greenblatt, D., "Plasma-based feed-forward dynamic stall control on a vertical axis wind turbine," *Wind Energy*, Vol. 19, No. 1, 2016, pp. 3-16. https://doi.org/10.1002/we.1814.
14. Garcia, M., Mongin, M. and Greenblatt, D., "Closed-loop stall control using pulsed DBD-plasma-actuation," AIAA Scitech Forum, 6-10 January 2025, Orlando, FL. https://doi.org/10.2514/6.2025-0034.